Title

Achieving Uniform Lithium Electrodeposition in Cross-Linked Poly(ethylene oxide) Networks: “Soft” Polymers Prevent Metal Dendrite Proliferation

Journal

Macromolecules, 53(13)

ISSN

0024-9297

Authors

Stalin, Sanjuna
Johnson, Hillis EN
Biswal, Prayag
et al.

Publication Date

2020-07-14

DOI

10.1021/acs.macromol.0c00475

Peer reviewed

Macromolecules

pubs.acs.org/Macromolecules Article

Achieving Uniform Lithium Electrodeposition in Cross-Linked Poly(ethylene oxide) Networks: "Soft" Polymers Prevent Metal Dendrite Proliferation

Sanjuna Stalin,[‖] Hillis E. N. Johnson,[‖] Prayag Biswal, Duylinh Vu, Qing Zhao, Jiefu Yin, Brooks A. Abel, Yue Deng, Geoffrey W. Coates,* and Lynden A. Archer*

Cite This: *Macromolecules* 2020, 53, 5445−5454 Read Online

ACCESS | Metrics & More | Article Recommendations | Supporting Information

ABSTRACT: The propensity of lithium to form nonplanar, mossy, or dendritic electrodeposits at current densities below the diffusion limit is a well-known, fundamental barrier to commercialization of energy-dense storage in lithium metal batteries. It has been proposed that proliferation of Li dendrites can be eliminated by controlling the uniformity and size of the deposits to levels where surface tension and other small-scale interfacial forces are able to planarize the deposition. Herein, we investigate lithium electrodeposition in uniformly porous, nanostructured media formed in cross-linked poly(ethylene oxide) polymer networks enabled by thiol−ene click chemistry. Using galvanostatic strip-plate experiments along with scanning electron microscopy and operando visualization techniques, we critically assess the effectiveness of these materials in enabling uniform, planar deposition of lithium. We report that thiol−ene click networks that host a liquid electrolyte in their pores are more effective than their liquid electrolyte or solid polymer network components in regulating Li deposition at both the nucleation and growth phases. It is shown further that compressive interfacial stresses imparted by the networks during electrodeposition may serve to augment surface tension to enable uniform Li electrodeposition. The practical relevance of these electrolytes is demonstrated in full-cell battery configurations with excellent long-term stability.

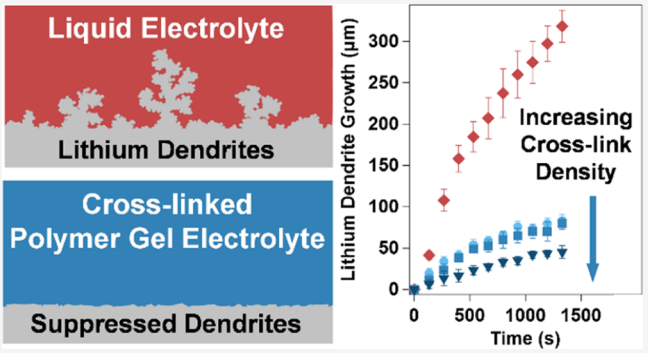

INTRODUCTION

Rechargeable lithium batteries have revolutionized consumer electronics and electric vehicle technology since their first successful commercialization by Sony in 1991. Configurations with lithium metal as the anode have attracted significant interest because of their high volumetric and gravimetric energy densities.[1−4] The commercialization of such lithium metal batteries (LMBs) has been hindered, however, by the notorious problem of unstable, nonplanar electrodeposition at the anode surface. This leads to formation of rough, mossy, or dendritic metal morphologies at the anode during battery recharge, which can lead to premature battery failure by a variety of mechanism.[5] Extensive research efforts have focused on the suppression of lithium dendrites by means of salt additives,[6,7] coatings on the lithium metal anode,[8−10] single ion conductors,[11−13] and high modulus solid-state electrolytes.[14−16] At current densities below the diffusion limit, the growth of Li dendrites is thought to occur in three stages.[17] The first stage involves the formation of a passivation layer by both chemical and electrochemical reduction of electrolyte components (such as solvents, salts, or additives) in contact with the electrode. This layer, termed the solid electrolyte interphase (SEI), was recently investigated by means of focused ion beam cryogenic scanning electron microscopy (SEM) and electron spectroscopy techniques and shown to be highly heterogeneous and far thicker than the analogous SEI formed on graphite anodes in lithium ion batteries (LIBs).[18] In the second stage, Li transport through the SEI produces heterogeneous deposits that lead to the nucleation of dendrites at zones of high conduction. Finally, the passivation layer may continuously break and reforms by reaction with the electrode and electrolyte, promoting continuous growth of the dendrites into ramified structures, with the growth direction determined by the least reactive crystallographic facet of metallic lithium.

On the basis of a linear stability analysis of electrodeposit growth on patchy metal nucleates, Tikekar et al. proposed that if the deposition of active metals could be limited to uniform nanoscale structures, interfacial forces such as surface tension,

Received: February 28, 2020
Revised: May 1, 2020
Published: June 30, 2020

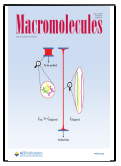

https://dx.doi.org/10.1021/acs.macromol.0c00475
Macromolecules 2020, 53, 5445−5454

Scheme 1. Synthesis of Cross-Linked Polymer Electrolytes Used in This Study

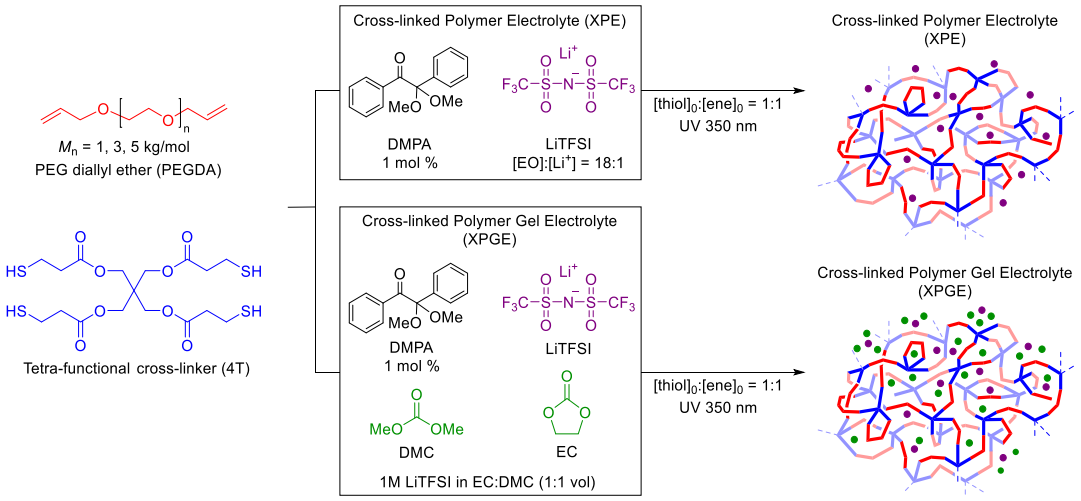

Table 1. Summary of Thermal and Conductive Properties of Solid Cross-Linked Networks

Network (XPE-*n*k)[a]	PEGDA M_n (kg/mol)[b]	T_g (°C)[c]	T_m (°C)[c]	T_c (°C)[c]	ΔH_{fus} (J/g)[c]	σ (S/cm) at 25 °C[d]	σ (S/cm) at 90 °C[d]
XPE-1k	1.0	−46	n.d.[e]	n.d.[e]	n.d.[e]	2.2×10^{-5}	4.3×10^{-4}
XPE-3k	3.0	−48	19	−6	43	5.4×10^{-5}	7.4×10^{-4}
XPE-5k	4.6	−45	31	2	57	3.5×10^{-5}	8.2×10^{-4}

[a]All films have an EO/Li ratio of 18:1 (r = 0.056), where EO denotes ethylene oxide units in the PEGDA. XPE-*n*k denotes cross-linked polymer electrolyte using PEGDA macromonomers of n kg/mol. [b]Number average molecular weight (M_n) determined by ^{1}H NMR. [c]Glass transition temperature (T_g), melting temperature (T_m), crystallization temperature (T_c), and enthalpy of fusion (ΔH_{fus}) were determined by DSC. [d]Determined by dielectric spectroscopy measurements. [e]Not detected.

which are strongest on small length scales, should be enough to prevent selective growth at the nucleates.[17,19] This implies that the resultant suppression of mossy or dendritic electrodeposition of metals could occur at much lower mechanical moduli than that predicted by Newman and Monroe.[20] Stabilization of lithium dendrites by confining deposition to nanoscales has been realized in inorganic nanostructured separators, such as alumina,[21] and cross-linked polymer electrolytes.[22−27,33] In the case of cross-linked polymer electrolytes, including both solvent-free membranes and gels,[28] the effect of the network nanostructure on dendrite growth is convoluted by the composition and heterogeneity of the SEI. It is therefore unclear which of these effects determines the effectiveness of cross-linked polymers in preventing proliferation of dendritic lithium.

This work was motivated by two recent developments that, when combined, enable rigorous evaluation of the effects of polymer networks on the morphology of metal electrodeposits in an intrinsically scalable materials chemistry platform. First, thiol−ene click chemistry has been demonstrated as a highly efficient method for the synthesis of cross-linked polymer networks with uniform mesh size distributions.[29,30] Second, in situ visualization of metal electrodeposition in galvanostatic strip-plate experiments performed using an optical microscope has emerged as a powerful tool for directly quantifying morphology evolution at a lithium electrode in real time.[5,31] Here, we use thiol−ene chemistry to cross-link macromonomers based on poly(ethylene oxide) (PEO) to create novel solid-state polymer electrolyte materials with exceptional electrochemical stability when in contact with a Li metal anode. Through simple adjustments of the synthesis conditions, we show further that it is possible to manipulate the network pore size, allowing us to precisely evaluate the effectiveness of the materials in preventing dendrite proliferation in galvanostatic visualization experiments. The results show that cross-linked polymer membranes are remarkable electrolytes, when used either as dry/solvent-free materials or as a gel host for a liquid electrolyte. Finally, the feasibility of these networks for high-voltage LMBs is demonstrated for broader applications.

RESULTS AND DISCUSSIONS

Previously, we reported the synthesis of cross-linked membranes based on Poly(ethylene glycol) dimethacrylate and PE-PEO.[22,23] In this work, cross-linked network films were synthesized using photoinitiated thiol−ene polymerization, as depicted in Scheme 1. Thiol−ene networks have several advantages, including efficient and uniform network formation, mild reaction conditions, tolerance to a variety of functional groups, and inexpensive commercial monomers.[29,30] Poly(ethylene glycol) diallyl ether macromonomer (PEGDA) was synthesized by reacting PEG diol with sodium hydride and allyl bromide (see Supporting Information for details). PEGDA was then mixed with tetra-thiol cross-linker (4T), photoinitiator (DMPA), and LiTFSI until homogeneous. A stoichiometric balance between $[thiol]_0$ and $[ene]_0$ contents was maintained for all samples. The concentration of lithium in each sample was determined by r, which is the molar ratio of lithium ions to ether oxygens ($[Li^+]/[EO]$). Samples used in this study used r = 0.056 ([Li]/[EO] = 1:18) unless otherwise noted. The mixture was then cast on silylated glass plates and cured under 350 nm UV light at 80 °C. A spacer was used to generate films of desired thickness (typically 100 μm). Cured films were characterized by Fourier transform infrared spectroscopy (Figure S3) to confirm the disappearance of thiol peaks at

https://dx.doi.org/10.1021/acs.macromol.0c00475
Macromolecules 2020, 53, 5445−5454

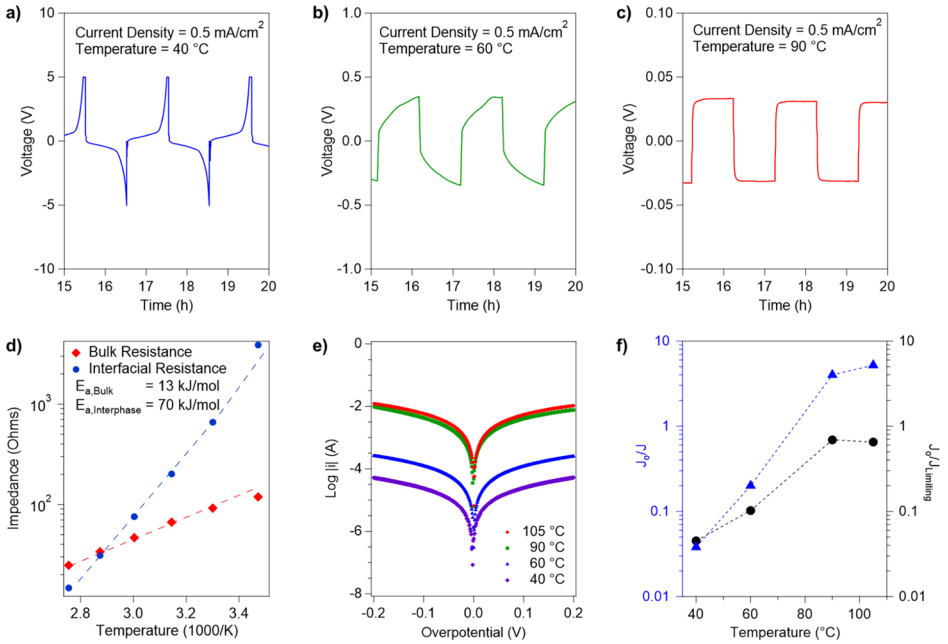

Figure 1. Galvanostatic strip-plate measurements using Li/XPE-3k/Li cells at (a) 40, (b) 60, and (c) 90 °C. (d) Impedance measurements showing bulk and interfacial impedances as a function of temperature. Fitting of raw data reveals higher activation energy for interfacial ion transport. (e) Current−overpotential plot measured by cyclic voltammetry of XPE-3k at different temperatures. (f) Exchange current density normalized to the current density of operation (blue) and to the limiting current (black) for XPE-3k as a function of temperature.

around 2550 cm^{-1}. Thermal properties were characterized by differential scanning calorimetry (DSC) and are reported in Table 1. The original traces are shown in Figure S4. Atomic force microscopy was used to observe the morphology and topography of the films. As seen in Figure S5, the cross-linked membranes are relatively homogenous with no prominent surface features. This conclusion is supported by phase mapping (Figure S5a). The cross-linked membrane with salt, however, showed some roughness and inhomogeneity. We hypothesized that this was due to salt aggregates which occur at room temperature from partial precipitation of the LiTFSI salt in the membrane. AFM phase contrast mapping reveals obvious spatial variations in the materials (Figure S5b).

Lithium ion transport is thought to occur predominately in the amorphous region of a polymer electrolyte, promoted by the segmental motion of polymer chains. As reported previously, cross-linking PEO chains will disrupt the formation of crystalline domains and increase the available amorphous volume for ion conduction.[22,24,27,32,33] To evaluate the effect of chain length between cross -links on ionic conductivity and electrolyte physical properties, PEGDA macromonomers of different molecular weights were synthesized and cross-linked into networks of varied cross-link density. Thermal properties and ionic conductivities for different networks are shown in Table 1. Ionic conductivities over a temperature range of −15 to 90 °C are reported in Figure S6. We observed that as molecular weight between cross-links increased, starting at approximately 3000 g/mol, a melting transition emerged. This value is comparable to the critical molecular weight, M_c, ($M_c \approx 2M_{entanglement}$ = 3248 g/mol)[34] at which intermolecular entanglements begin to dominate transport properties in PEO. This suggests that there is a competition between chain mobility and crystallization with varying molecular weights. In other words, at high cross-link densities, low segmental motion and a denser network impair ion transport. Accordingly, because cross-link density and PEO molecular weight are inversely coupled for the networks studied, a maximum in conductivity was observed for networks comprised of PEO macromonomers of M_n near M_c. We note that the conductivity maximum was also observed at a similar molecular weight for other cross-linked systems based on PEO and LiTFSI salt, regardless of the cross-linking chemistry utilized.[22,23] This is consistent with the idea that this molecular weight is a fundamental characteristic of cross-linked PEO networks associated with M_c. For subsequent studies reported in the article, we therefore focus on networks using 3000 g/mol PEO-based macromonomers because of their high conductivity at room temperature and above relative to the other networks.

One of the main motivations for using a cross-linked polymer electrolyte is to evaluate the predictions of recent theory that such materials may be able to confine electrodeposition of metals to small length scales proportional to the cross-link density or mesh size of the network. To characterize the average mesh size of the networks, rheological measurements were performed at different temperatures. Dynamic storage (G') and loss (G'') moduli measured in small strain amplitude (strain = 0.1%) oscillatory shear measurements in the linear viscoelastic regime are reported in Figure S7a, and a direct comparison with XPE-1k and XPE-5k is presented in Figure S7b. It is evident that the G' values are nearly independent of frequency and almost 2 orders of magnitude higher than G'', indicating the elastomeric nature of the electrolytes. The high-frequency storage modulus value, G_e, increases with increasing cross-link density as expected. G_e also increased with increasing absolute temperature, with typical values ranging from 0.4 MPa (at 40 °C) to 0.85 MPa (at 90 °C) for XPE-3k. This allows an estimation of the average mesh size, a, of the networks using the following equation[34]

$$a = \sqrt[3]{\frac{kT}{G_e}} \quad (1)$$

https://dx.doi.org/10.1021/acs.macromol.0c00475
Macromolecules 2020, 53, 5445−5454

The calculated values are in the range 1−5 nm for the three systems, indicating that the networks are tightly cross-linked. Alternatively, the measured G'' can be used to obtain an empirical value for the molecular weight between cross-links, M_x, using the relationship

$$M_x = \frac{\rho RT}{G_e} \quad (2)$$

where $\rho = \rho_{network} \approx 1.2$ g/cm^3 and $G_e \approx 2$, 0.9, and 0.5 MPa at 90 °C for XPE-1k, XPE-3k, and XPE-5k, respectively (see Figure S7b). The obtained values for M_x—1600, 3500, and 6100 g/mol for XPE-1k, XPE-3k, and XPE-5k, respectively—closely agree with the predicted values for a highly uniform cross-linked network of PEO chains, further showing the precision of thiol−ene click chemistry used for the XPE synthesis.

To evaluate the effectiveness of our cross-linked polymer electrolytes in stabilizing electrodeposition, we first performed galvanostatic strip-plate measurements at 40, 60, and 90 °C using the solid-state XPE-3k. We note that these materials contain no solvent or plasticizer. Figure S8 shows the voltage responses at different temperatures for a sequence of 1 h plating and stripping experiments. At 60 °C, the overpotentials are high (~0.5 V), but the materials exhibit stable cycling profiles for over 100 cycles (200 h). At 90 °C, the overpotentials are substantially lower (0.04 V); however, despite stable initial cycling, the cells quickly fail. Figure 1a−c shows magnified versions of the profiles for each temperature. The initial voltage response at 90 °C is notable for its square-wave shape, which exactly tracks the imposed current. This feature is not found in liquid electrolytes and appears to be characteristic for solid-state electrolytes.[35,36] In the case of liquid electrolytes, Dasgupta and co-workers proposed that the sharp voltage extrema observed during the onset of Li plating and stripping are associated, respectively, with formation of mossy dendrites and pitting at the electrode surface.[5,32,33] These designations have recently been confirmed in direct optical visualization studies for sodium metal anodes,[37] indicating that the nearly Ohmic voltage response observed from the XPEs is associated with suppression of mossy dendrite formation and pitting. The large transient overpotentials at 40 °C disappear at 90 °C. We hypothesize that ion transport "bottlenecks", where the high interfacial resistance (much larger in magnitude than the bulk resistance), is the source of this observation. In liquid electrolytes, a higher interfacial resistance to ion transport arises from slower, solid-state ion transport in the SEI. For cross-linked polymer electrolytes, the difference could arise either from electrochemical reduction of the electrolyte to form an SEI or poor interfacial contact with the electrode.

Figure 1d reports the bulk and interfacial resistances of the cross-linked polymer electrolytes obtained by fitting the temperature-dependent impedance data in Figure S9. The cells were rested at 80 °C for 3 h before measuring the impedance. It is noted here that the interfacial resistance includes contributions from the SEI formed on the electrode and the extent of interfacial contact between the solid electrolyte and the electrode, which is more conformal at higher temperatures. The results show that the interfacial resistance is generally much larger than the bulk resistance, particularly at lower temperatures. Vogel−Tammann−Fulcher fits to the data show that the activation energy for the interface transport process is also substantially larger; implying that the higher interfacial resistance arises from slower ion transport at the polymer−Li interface in comparison to the electrolyte bulk. At temperatures above 70 °C, the interfacial resistance becomes lower than the bulk resistance. The transition to faster interfacial ion transport coincides with our observations of square-wave like profiles at 90 °C, supporting the hypothesis that deviations of the voltage response from the imposed current profile in a strip-plate experiment originates from ion transport "bottlenecks" at the interface. However, at higher temperatures, the cells unexpectedly failed faster. The voltage profiles at 90 and 105 °C for cells polarized at 0.5 mA/cm^2 show that the cells failed four times faster at the higher temperature, despite the increase in network modulus with temperature (Figure S10). To gain insights into the underlying phenomena, we used cyclic voltammetry to measure the exchange current density, J_o, at Li/XPE-3k interfaces over the same range of temperatures (see Supporting Information for details). The current-overpotential plot (Figure 1e) shows an increase in the exchange current with temperature, particularly in the range 60 to 90 °C. Figure 1f reports exchange current density, J_o, values for the Li/XPE-3k interface, normalized by the current density, J, at which the cell was operated (0.5 mA/cm^2). It is apparent that J_o is not only a strongly increasing function of temperature, but that the strongest increase (nearly 2 orders of magnitude) occurred over a narrow temperature range that correlates more closely with the normal melting transition temperature ($T_m \approx 60$ °C) of non-cross-linked or loosely cross-linked high molecular weight PEO. This is potentially due to a lower degree of cross-linking at the surface of the XPE compared to the bulk. We further note that the large increase in J_o coincided with very large reductions in the interface resistance (Figure 1d) and commensurately lower overpotentials in the Li plate-strip experiment. We attribute both observations to improved interfacial contact between the solid polymer electrolyte and the Li metal electrode. It is also apparent that at temperatures above approximately 70 °C, $J_o \gg J$, meaning that the electrode reaction becomes transport limited—a requirement for rapid dendrite growth.[38] We measured the limiting current density, $J_{limiting}$, using a combination of current−voltage measurements (see Figure S11) and calculations. Normalizing J_o by the temperature-dependent $J_{limiting}$ values (see Figure 1f, right axis) shows that the kinetics of the Li reduction reaction at the anode increase more rapidly with temperature than the bulk diffusivity of the electrolyte, leading to the same conclusion that the electrode reaction in the solid XPE electrolyte becomes progressively more transport limited at elevated temperatures. Thus, we conclude that the faster failure of the XPE electrolyte at higher temperatures was due to increased Li reduction kinetics, which resulted in dendrite growth. The mechanical properties of the cross-linked networks at these higher temperatures were insufficient to suppress the dendrites. These findings suggest that systems where the rate of reduction at the electrode surface is lower than the driving current should lead to an increase in the concentration of ions at the electrode surface, stabilizing deposition. This can be achieved by increasing the bulk conductivity and lowering the temperature of operation in the system.

To overcome transport limitations of the solid XPE electrolytes for room temperature operation, the cross-linked polymer networks were soaked in liquid electrolyte to increase their bulk and interfacial ionic conductivities. We used a liquid electrolyte composed of 1 M LiTFSI dissolved in a 1:1 (v/v)

https://dx.doi.org/10.1021/acs.macromol.0c00475
Macromolecules 2020, 53, 5445−5454

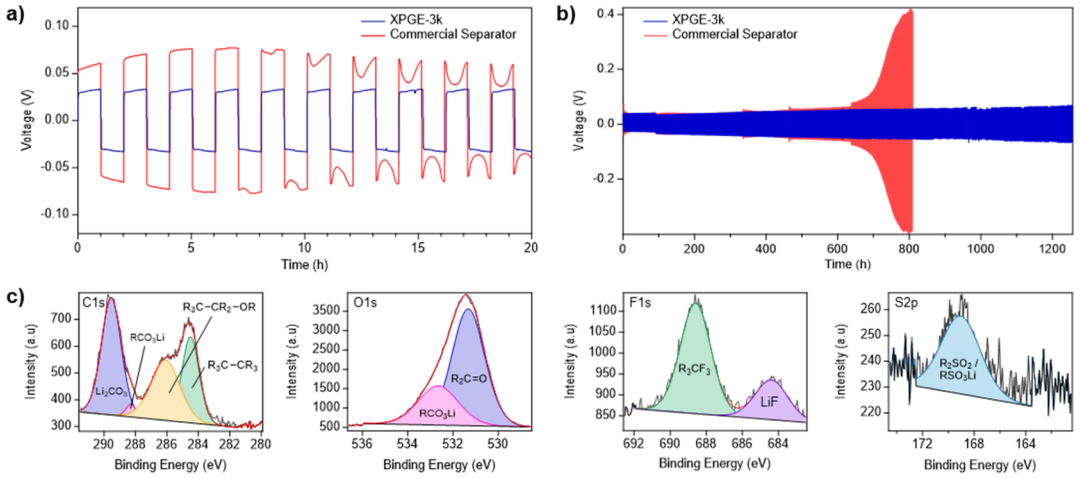

Figure 2. Lithium deposition behavior in a cross-linked polymer gel electrolyte (XPGE-3k) network at room temperature (22 °C). Tests were performed at a current density of 0.5 mA/cm^2 which include one-hour stripping and plating cycles. (a) Magnified profiles in the first 20 h compared to a commercial separator (Celgard 3501). (b) Long-term stability of the XPGE-3k network. (c) XPS analysis of the SEI formed with XPGE-3k against the lithium metal anode. Analysis reveals SEIs are mainly formed from the decomposition of LiTFSI and EC/DMC.

mixture of ethylene carbonate (EC) and dimethyl carbonate (DMC) in all studies. The cross-linked networks swelled by an average of 40−60% by mass in the liquid electrolyte. The resulting materials obtained after maximum electrolyte uptake were mechanically tough, elastic materials with G_e values comparable to those of the original XPEs (Figure S12). Remarkably, however, the room temperature ionic conductivity of the materials was much higher (on the order of 10 mS/cm, i.e., 3 orders of magnitudes higher than the solid XPEs at 90 °C, Figure S13). We term the materials cross-linked gel electrolyte (XPGE) membranes because they host the liquid electrolyte within the network; their mechanics are, however, similar to those of the solid XPEs. These features validate the uniformity of the cross-linking (few unlinked/dangling chains) present in the XPEs.

Electrochemical impedance spectroscopy measurements indicated that the liquid component in the XPGEs drastically reduced the interfacial resistance at room temperature to values comparable to those of the solid XPEs at 90 °C (Figure S14). We suspect this arises from improved interfacial contact between the electrolyte and the electrode. Room-temperature galvanostatic strip-plate experiments were performed for the XPGEs at a current density of 0.5 mA/cm^2. Figure 2a reports the voltage response of XPGE-3k along with a control composed of the same liquid electrolyte infused in a 25 μm thick porous polyolefin (Celgard 3501) separator (expanded plots of the voltage response are shown in Figure S15). The control electrolyte showed the typical large voltage overpotentials associated with pitting and stripping of lithium from underneath electrochemically disconnected mossy deposits. These features are absent in the XPGE-3k material. The voltage profile of XPGE-3k at 22 °C instead resembles the square-wave response previously observed in the solid polymer system (XPE) at 90 °C, indicating that pitting is suppressed. Galvanostatic cycling at a higher current density of 1 mA/cm^2 revealed similar square-wave like profiles (Figure S16).

In order to eliminate the effect of thickness differences between XPGE-3k and the Celgard control, additional polarization experiments at 1 mA h/cm^2 were performed with glass fiber separators. The glass fiber separators were the same thickness as XPGE-3k (100 μm) and were soaked in the same electrolyte. Figure S17 shows that XPGE-3k is nearly twice as effective as the glass fiber separator in resisting failure by short-circuit. Our results therefore imply that cross-linked polymer gels are effective in preventing mossy lithium electrodeposition, orphaning of the mossy lithium deposits, or both. Figure 2b reports the voltage profiles obtained from long-term strip-plate cycling experiments. The XPGE-3k cell showed superior cyclability relative to XPE-3k and was able to maintain stable cycling with minimal potential drift for more than 1000 h (>600 cycles). In comparison, the control cells in which the same liquid electrolyte was hosted in a commercial polyolefin separator failed after ∼800 h (400 cycles). XPS analysis of the lithium metal anode surface after cycling with XPGE-3k showed that the SEI was primarily composed of carbonates and lithium fluoride salts (Figure 2c). The distribution of byproducts was similar to that found in typical carbonate-based electrolytes, implying that they arose primarily from decomposition of the liquid carbonate and LiTFSI salt (Figure S18). On this basis, we concluded that better interface contact and not the SEI composition is the likely source of the enhanced stability of the XPGE-3k electrolyte.

To study the morphology of lithium deposits at early stages of deposition, a small capacity of lithium (0.1 mA h/cm^2) was deposited on a stainless-steel substrate in cells containing XPGE-3k and compared to cells containing a Celgard 3501 separator as a control. SEM analysis of the deposits revealed that the average diameter of Li nuclei formed in the XPGE-3k electrolytes were much smaller (0.14 μm in XPGE-3k compared to 0.96 μm in Celgard) and the number density of nuclei were correspondingly larger (5.9 vs 0.27 nuclei/μm^2) (Figure 3). Using eq 1 and the measured moduli for the XPGE electrolytes (see Figure S12), we estimate the network mesh diameter of XPGE-3k to be at most 5 nm, which is evidently much smaller than the average nuclei diameter, confounding any straightforward relationship between the network structure and nucleate size.

In order to determine the cause of the different Li morphologies, we first consider the mechanism of Li nucleation. Metal nucleation at lower areal capacities is characterized by a nucleation overpotential, while the subsequent growth at higher areal capacities is dominated by

https://dx.doi.org/10.1021/acs.macromol.0c00475
Macromolecules 2020, 53, 5445−5454

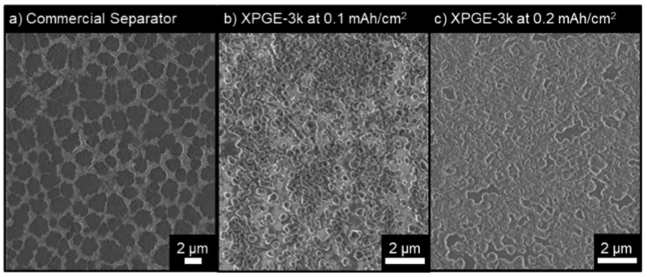

Figure 3. SEM analysis of lithium nucleation and growth in a commercial separator vs the XPGE-3k network. (A) Average nuclei size: 0.96 μm. Nuclei density: 0.27 nuclei/μm^2. (b) Average nuclei size: 0.14 μm. Nuclei density: 5.9 nuclei/μm^2. (c) Average nuclei size: 0.20 μm. Nuclei density: 8.5 nuclei/μm^2.

mass transfer overpotentials.[36] A sharp peak in the voltage response marks the nucleation overpotential, while the later gradual plateauing of the voltage response to lower voltage indicates the transition to mass transfer overpotentials. In Figure S19, the nucleation overpotential can be identified at areal capacities of approximately 0.03 mA h/cm^2 for both the Celgard separator and the XPGE-3k. The voltage response for the commercial separator gradually plateaus to a lower voltage at higher capacities. Surprisingly, the XPGE networks showed no plateauing transition in voltage response to the mass transfer-controlled zone, even at higher capacities. The nucleation overpotential is a consequence of an interplay between activation and nuclei surface formation. The activation overpotential can be interpreted as the charge-transfer overpotential because of the heterogeneous nature of electrodeposition at the interface of the liquid bulk electrolyte and a solid stainless-steel current collector. On the other hand, the nuclei surface formation overpotential is a consequence of the extra energy required to grow nuclei. For the XPGE networks, we observed that the nuclei density and average nuclei size increased with increasing electrodeposited areal capacity (Figure 3b,c). Coalescence of lithium nuclei was also observed as areal capacity increased. This indicates that simultaneous progressive nucleation, growth, and agglomeration are all contributing to the plateau overpotential. The smaller lithium nuclei supported in the elastic polymer framework would maintain better contact with the interface, facilitating more efficient electron transport and reversibility of the lithium deposition. The larger number density is also potentially beneficial as it would lead to a higher probability of merging of nuclei to produce the flatter electrodeposit profiles observed by SEM analysis.

At least two hypotheses can therefore be proposed to explain the effectiveness of cross-linked polymers in facilitating stable lithium electrodeposition. First, consistent with the linear stability analysis reported by Tikekar et al.,[17,19] the smaller

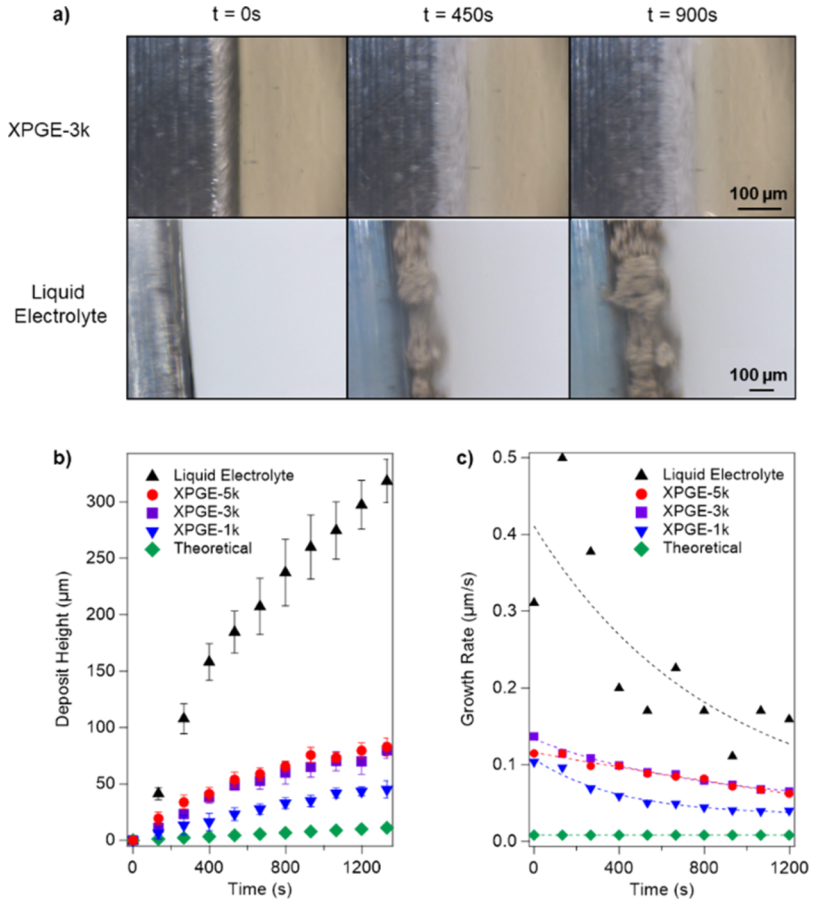

Figure 4. Visualization of lithium deposition. (a) Comparison of deposition in a cross-linked polymer gel electrolyte (XPGE) and liquid electrolyte [1 M LiTFSI in 1:1 (v/v) EC/DMC] at J = 6 mA/cm^2. (b) Analysis of electrodeposit height at J = 6 mA/cm^2 for the liquid electrolyte and XPGE networks. (c) Growth rate as a function of time compared to theoretical predicted values estimated from the current density and capacity of lithium deposited.

https://dx.doi.org/10.1021/acs.macromol.0c00475
Macromolecules 2020, 53, 5445−5454

pore size of the cross-linked polymer, in comparison to Celgard, could amplify the effect of forces, such as surface tension, that are strongest on small length scales in preventing rapid growth of nuclei. Alternatively, the mechanical stresses produced by the cross-linked polymer membrane in contact with the growing nuclei will exert a local tensile force on the growing nuclei that is analogous to surface tension.[19] This force will augment normal surface tension by an amount proportional to the shear modulus of the polymer network and would produce a planarizing effect on the Li nuclei analogous to what is observed in the experiments.

To evaluate these hypotheses, direct operando visualization experiments were performed at fixed current densities to visualize time-dependent morphology changes at the Li anode during continuous plating/polarization. Figure 4a shows the results from a visualization experiment performed at 6 mA/cm^2. The Li deposits in XPGE-3k are notably more uniform and less mossy in comparison to the carbonate-based liquid electrolyte. Results for analogous visualization experiments using XPGE-5k and XPGE-1k are reported in Figure S20. These results also show that the morphology is consistently more compact when electrodeposition of Li is performed in the cross-linked polymer electrolytes.

The average electrodeposit thickness and growth rate at 6 mA/cm^2 were analyzed using MATLAB to gain insights into the evolution of lithium electrodeposition. Multiple points on the propagating front were tracked and averaged to obtain plots of the deposit height and growth rate over time for XPGE-1k, XPGE-3k, XPGE-5k, and a liquid electrolyte (1 M LiTFSI in EC/DMC) (Figure 4b,c). As evident from Figure 4b, the lithium deposit thickness increases more slowly in the XPGE electrolytes, in comparison to just the liquid electrolyte. The rate at which the electrodeposit thickness increases also varied with cross-link density, with higher cross-link density (i.e., lower PEO MW) networks resulting in slower growth (Figure 4c). Additionally, the standard deviation in the electrodeposit thickness at each time point provides information about the spatial variation in growth rates of the propagating deposit front. Notably, all XPGE networks show narrow deviations in deposit height and thus more uniform lithium deposition. However, we note that the suppressed growth rates in the cross-linked membranes are still substantially higher than expected for a lithium metal layer with density equal to that of the bulk metal. This indicates that while electrodeposition of lithium in the cross-linked polymers is more compact than in the liquid electrolyte, the electrodeposit structures are less dense than the bulk metal.

In all cases, it was observed that the Li deposit growth rate decreased before reaching a constant value. It is possible that stress develops in the cross-linked network over time due to lithium deposition, eventually reaching a saturation point, which produces a constant, lower growth rate. To test this idea, a mechanical rheology experiment was designed to model the conditions of the visualization experiment and the deposition process (Figure S21). A sample of XPGE-3k was compressed between assymmetric parallel plates in a mechanical rheometer equipped with a custom-made upper parallel plate with a diameter of 1.5 mm and a lower plate at least 10-times larger. The upper plate was driven downward at a constant normal velocity and the force per unit area measured. The information was used to obtain the transient compressive stress in the network. As can be seen in Figure 5a, the compressive stress on the networks saturated at a high stress value before eventual

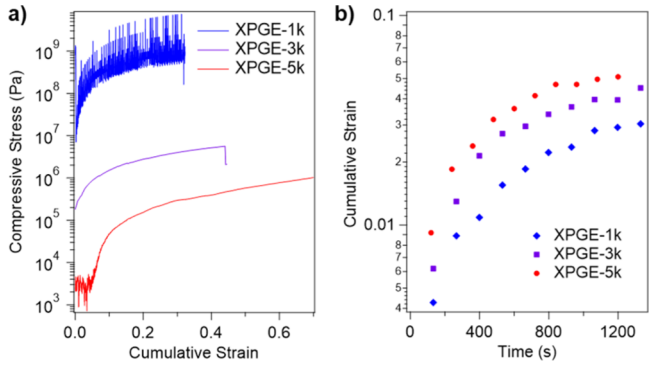

Figure 5. Rheological responses of the cross-linked polymer to dendritic growth. (a) Compressive stress as a function of strain for the XPGE networks. (b) Cumulative strain experienced by the XPGE networks during dendrite propagation in the visualization experiment.

material failure was observed. XPGE networks comprising higher cross-link densities (lower molecular weight between cross-links) produced stress values orders of magnitude higher than lower cross-link density networks, offering a plausible explanation for the suppressed Li deposit growth rates observed for XPGE-1k. The experiment was also performed at three different compression velocities for each XPGE network (Figure S22). For each network, the compressive stress increased moderately with higher compression velocity. This was likely due to easier deformation of polymer segments, which then exerted higher elastic forces to resist deformation on shorter time scales. The yield strain value deduced from the compression experiments also decreased as cross-link density increased.

In order to compare the model compression experiment to the visualization studies, the strain experienced by the polymer networks during deposition was calculated from the visualization experiments (Figure 5b). At about 600 s, the cumulative strain in the networks began to plateau. This would increase the effective modulus experienced by the lithium deposits and lead to reduced growth rates on similar timescales. Results reported in Figure 4c show that the lithium deposit growth rate also approached steady state within approximately 600 s. Thus, the effective suppression of dendritic propagation of lithium by cross-linked polymers may be due to the high levels of compressive stress developed in the network as the dendrites propagate.

Finally, to assess the potential for wider applications of cross-linked polymer gel electrolytes for practical LMBs, we assembled Li||NCM 622 cells with high cathode loadings (3 mA h/cm^2) and XPGE-3k as the electrolyte. Ether-based electrolytes are known to decompose at high voltages but can be stabilized by lithium bis(oxalato)borate (LiBOB) salts owing to the formation of a protective cathode-electrolyte interface (CEI).[39] To create a similarly stable CEI, the porous cathode was wetted with a LiBOB-containing liquid electrolyte (0.4 M LiBOB, 0.6 M LiTFSI, 0.05 M $LiPF_6$ in 1:1 (v/v) EC/DMC) prior to cell assembly. $LiPF_6$ is included in the formulation to prevent corrosion of the aluminum current-collector used for the cathode. XPGE-3k was used as the bulk electrolyte without modifying its previously described composition. Cycling results for a control cell containing only the liquid electrolyte is included for comparison in Figure S23. We note that the XPGE-3k cell has a higher capacity retention compared to the control cell. The cycling results

https://dx.doi.org/10.1021/acs.macromol.0c00475
Macromolecules 2020, 53, 5445−5454

showed excellent active material utilization and capacity retention at a moderate rate of C/5 for over 120 cycles (Figure 6a). The corresponding voltage profiles in Figure 6b show a high coulombic efficiency of >99.5% and no signs of electrolyte decomposition.

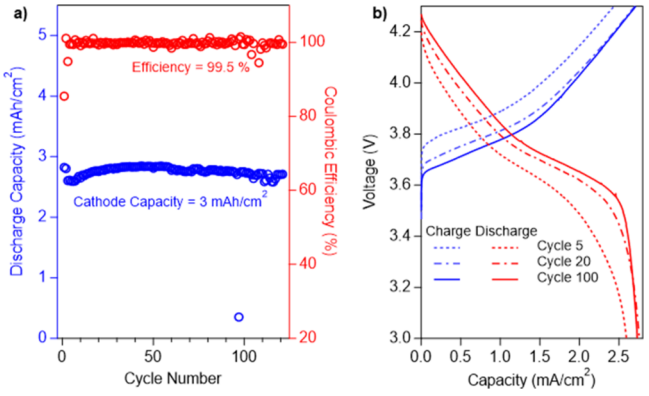

Figure 6. (a) Full-cell cycling results at a rate of C/5. (b) Voltage profiles for the 5th, 20th and 100th cycles. Cells were constructed using a 750 μm thick lithium metal anode, XPGE-3k electrolyte, and an NCM 622 cathode previously wetted by a carbonate electrolyte based on EC/DMC with LiTFSI, LiBOB, and $LiPF_6$ salts.

CONCLUSIONS

We have synthesized highly uniform PEO-based networks using thiol−ene chemistry in order to study lithium electrodeposition in cross-linked polymer electrolyte networks. Conductivity measurements of the solid polymer networks in this study indicated a critical molecular weight of PEO chains at which maximum conductivity was achieved. Galvanostatic strip-plate experiments and impedance measurements showed stable solid-state cycling as a result of low interfacial resistance at high temperatures. However, investigation into the interplay between lithium ion diffusion through the network and the reaction rate at the electrode interface using cyclic voltammetry suggests that the ratio between diffusion and reaction rate is a crucial factor to consider in the design of cross-linked polymer electrolytes.

Soaking the polymer networks in a liquid electrolyte to form XPGE networks improved lithium ion diffusion and interfacial kinetics. Notably, the XPGE networks showed stable cycling in excess of 150 cycles despite hosting a liquid electrolyte known to decompose at the electrode over time. Optical microscopy in operando visualization techniques showed that the XPGE networks are capable of significant suppression of lithium dendrite growth by enabling controlled, uniform lithium deposition. SEM analysis of the lithium anode surface further revealed that the network architecture enabled small, dense lithium deposits in the initial phase of nucleation. As deposition progressed, the nuclei were found to merge and form planar deposits. Additionally, the effect of cross-link density and subsequently the compressive stresses developed in the networks during electrodeposition were also investigated using rheology. It was found that the compressive stresses in the networks play a key role in the suppression and saturation of the growth rate of lithium deposits over time, possibly leading to the observed planar deposits. Finally, the practical applicability of these electrolytes was demonstrated in full cell LMB configurations with excellent long-term stability over 100 cycles.

ASSOCIATED CONTENT

Supporting Information

The Supporting Information is available free of charge at https://pubs.acs.org/doi/10.1021/acs.macromol.0c00475.

Experimental procedures, characterization data, and spectra of all compounds synthesized in this study and electrochemical characterization data and rheology data of the cross-linked polymer electrolytes (PDF)

AUTHOR INFORMATION

Corresponding Authors

Geoffrey W. Coates − *Department of Chemistry and Chemical Biology, Baker Laboratory, Cornell University, Ithaca, New York 14853, United States;* orcid.org/0000-0002-3400-2552; Email: gc39@cornell.edu

Lynden A. Archer − *School of Chemical and Biomolecular Engineering, Cornell University, Ithaca, New York 14853, United States;* orcid.org/0000-0001-9032-2772; Email: laa25@cornell.edu

Authors

Sanjuna Stalin − *School of Chemical and Biomolecular Engineering, Cornell University, Ithaca, New York 14853, United States;* orcid.org/0000-0002-4786-6640

Hillis E. N. Johnson − *Department of Chemistry and Chemical Biology, Baker Laboratory, Cornell University, Ithaca, New York 14853, United States;* orcid.org/0000-0002-5998-9234

Prayag Biswal − *School of Chemical and Biomolecular Engineering, Cornell University, Ithaca, New York 14853, United States*

Duylinh Vu − *School of Chemical and Biomolecular Engineering, Cornell University, Ithaca, New York 14853, United States*

Qing Zhao − *School of Chemical and Biomolecular Engineering, Cornell University, Ithaca, New York 14853, United States*

Jiefu Yin − *School of Chemical and Biomolecular Engineering, Cornell University, Ithaca, New York 14853, United States*

Brooks A. Abel − *Department of Chemistry and Chemical Biology, Baker Laboratory, Cornell University, Ithaca, New York 14853, United States;* orcid.org/0000-0002-2288-1975

Yue Deng − *Department of Materials Science and Engineering, Cornell University, Ithaca, New York 14853, United States*

Complete contact information is available at: https://pubs.acs.org/10.1021/acs.macromol.0c00475

Author Contributions

‖S.S. and H.E.N.J. contributed equally.

Notes

The authors declare no competing financial interest.

ACKNOWLEDGMENTS

We thank the Beijing Institute of Collaborative Innovation for financial support of this study. The work made use of materials characterization facilities in the Cornell Energy Systems Institute (CESI), Cornell Center for Materials Research (CCMR), and the Cornell University NMR Facility. CCMR is supported by the National Science Foundation MRSEC program (award number: DMR-1719875) and the NMR

https://dx.doi.org/10.1021/acs.macromol.0c00475
Macromolecules 2020, 53, 5445−5454

facility is supported in part through NSF award number CHE-1531632.

REFERENCES

(1) Goodenough, J. B. Rechargeable Batteries: Challenges Old and New. *J. Solid State Electrochem.* **2012**, *16*, 2019−2029.
(2) Goodenough, J. B.; Park, K.-S. The Li-Ion Rechargeable Battery: A Perspective. *J. Am. Chem. Soc.* **2013**, *135*, 1167−1176.
(3) Armand, M.; Tarascon, J.-M. Building Better Batteries. *Nature* **2008**, *451*, 652−657.
(4) Tarascon, J.-M.; Armand, M. Issues and Challenges Facing Rechargeable Lithium Batteries. *Nature* **2001**, *414*, 359−367.
(5) Wood, K. N.; Noked, M.; Dasgupta, N. P. Lithium Metal Anodes: Toward an Improved Understanding of Coupled Morphological, Electrochemical, and Mechanical Behavior. *ACS Energy Lett.* **2017**, *2*, 664−672.
(6) Choudhury, S.; Archer, L. A. Lithium Fluoride Additives for Stable Cycling of Lithium Batteries at High Current Densities. *Adv. Electron. Mater.* **2016**, *2*, 1500246.
(7) Lu, Y.; Tu, Z.; Archer, L. A. Stable Lithium Electrodeposition in Liquid and Nanoporous Solid Electrolytes. *Nat. Mater.* **2014**, *13*, 961−969.
(8) Liu, K.; Pei, A.; Lee, H. R.; Kong, B.; Liu, N.; Lin, D.; Liu, Y.; Liu, C.; Hsu, P.-C.; Bao, Z.; Cui, Y. Lithium Metal Anodes with an Adaptive "Solid-Liquid" Interfacial Protective Layer. *J. Am. Chem. Soc.* **2017**, *139*, 4815−4820.
(9) Lopez, J.; Pei, A.; Oh, J. Y.; Wang, G.-J. N.; Cui, Y.; Bao, Z. Effects of Polymer Coatings on Electrodeposited Lithium Metal. *J. Am. Chem. Soc.* **2018**, *140*, 11735−11744.
(10) Choudhury, S.; Tu, Z.; Stalin, S.; Vu, D.; Fawole, K.; Gunceler, D.; Sundararaman, R.; Archer, L. A. Electroless Formation of Hybrid Lithium Anodes for Fast Interfacial Ion Transport. *Angew. Chem., Int. Ed.* **2017**, *56*, 13070−13077.
(11) Schaefer, J. L.; Yanga, D. A.; Archer, L. A. High Lithium Transference Number Electrolytes via Creation of 3-Dimensional, Charged, Nanoporous Networks from Dense Functionalized Nanoparticle Composites. *Chem. Mater.* **2013**, *25*, 834−839.
(12) Bouchet, R.; Maria, S.; Meziane, R.; Aboulaich, A.; Lienafa, L.; Bonnet, J.-P.; Phan, T. N. T.; Bertin, D.; Gigmes, D.; Devaux, D.; Denoyel, R.; Armand, M. Single-Ion BAB Triblock Copolymers as Highly Efficient Electrolytes for Lithium-Metal Batteries. *Nat. Mater.* **2013**, *12*, 452−457.
(13) Tu, Z.; Choudhury, S.; Zachman, M. J.; Wei, S.; Zhang, K.; Kourkoutis, L. F.; Archer, L. A. Designing Artificial Solid-Electrolyte Interphases for Single-Ion and High-Efficiency Transport in Batteries. *Joule* **2017**, *1*, 394−406.
(14) Yang, C.; Zhang, L.; Liu, B.; Xu, S.; Hamann, T.; McOwen, D.; Dai, J.; Luo, W.; Gong, Y.; Wachsman, E. D.; Hu, L. Continuous Plating/Stripping Behavior of Solid-State Lithium Metal Anode in a 3D Ion-Conductive Framework. *Proc. Natl. Acad. Sci. U.S.A.* **2018**, *115*, 3770−3775.
(15) Porz, L.; Swamy, T.; Sheldon, B. W.; Rettenwander, D.; Frömling, T.; Thaman, H. L.; Berendts, S.; Uecker, R.; Carter, W. C.; Chiang, Y.-M. Mechanism of Lithium Metal Penetration through Inorganic Solid Electrolytes. *Adv. Energy Mater.* **2017**, *7*, 1701003.
(16) Duan, H.; Yin, Y.-X.; Shi, Y.; Wang, P.-F.; Zhang, X.-D.; Yang, C.-P.; Shi, J.-L.; Wen, R.; Guo, Y.-G.; Wan, L.-J. Dendrite-Free Li-Metal Battery Enabled by a Thin Asymmetric Solid Electrolyte with Engineered Layers. *J. Am. Chem. Soc.* **2018**, *140*, 82−85.
(17) Tikekar, M. D.; Choudhury, S.; Tu, Z.; Archer, L. A. Design Principles for Electrolytes and Interfaces for Stable Lithium-Metal Batteries. *Nat. Energy* **2016**, *1*, 16114.
(18) Zachman, M. J.; Tu, Z.; Choudhury, S.; Archer, L. A.; Kourkoutis, L. F. Cryo-STEM Mapping of Solid−Liquid Interfaces and Dendrites in Lithium-Metal Batteries. *Nature* **2018**, *560*, 345−349.
(19) Tikekar, M. D.; Archer, L. A.; Koch, D. L. Stabilizing Electrodeposition in Elastic Solid Electrolytes Containing Immobilized Anions. *Sci. Adv.* **2016**, *2*, No. e1600320.
(20) Monroe, C.; Newman, J. The Impact of Elastic Deformation on Deposition Kinetics at Lithium/Polymer Interfaces. *J. Electrochem. Soc.* **2005**, *152*, A396.
(21) Tu, Z.; Zachman, M. J.; Choudhury, S.; Wei, S.; Ma, L.; Yang, Y.; Kourkoutis, L. F.; Archer, L. A. Nanoporous Hybrid Electrolytes for High-Energy Batteries Based on Reactive Metal Anodes. *Adv. Energy Mater.* **2017**, *7*, 1602367.
(22) Khurana, R.; Schaefer, J. L.; Archer, L. A.; Coates, G. W. Suppression of Lithium Dendrite Growth Using Cross-Linked Polyethylene/Poly(Ethylene Oxide) Electrolytes: A New Approach for Practical Lithium-Metal Polymer Batteries. *J. Am. Chem. Soc.* **2014**, *136*, 7395−7402.
(23) Stalin, S.; Choudhury, S.; Zhang, K.; Archer, L. A. Multifunctional Cross-Linked Polymeric Membranes for Safe, High-Performance Lithium Batteries. *Chem. Mater.* **2018**, *30*, 2058−2066.
(24) Choudhury, S.; Mangal, R.; Agrawal, A.; Archer, L. A. A Highly Reversible Room-Temperature Lithium Metal Battery Based on Crosslinked Hairy Nanoparticles. *Nat. Commun.* **2015**, *6*, 10101.
(25) Choudhury, S.; Vu, D.; Warren, A.; Tikekar, M. D.; Tu, Z.; Archer, L. A. Confining Electrodeposition of Metals in Structured Electrolytes. *Proc. Natl. Acad. Sci. U.S.A.* **2018**, *115*, 6620−6625.
(26) Lu, Q.; He, Y.-B.; Yu, Q.; Li, B.; Kaneti, Y. V.; Yao, Y.; Kang, F.; Yang, Q.-H. Dendrite-Free, High-Rate, Long-Life Lithium Metal Batteries with a 3D Cross-Linked Network Polymer Electrolyte. *Adv. Mater.* **2017**, *29*, 1604460.
(27) Duan, H.; Yin, Y.-X.; Zeng, X.-X.; Li, J.-Y.; Shi, J.-L.; Shi, Y.; Wen, R.; Guo, Y.-G.; Wan, L.-J. In-Situ Plasticized Polymer Electrolyte with Double-Network for Flexible Solid-State Lithium-Metal Batteries. *Energy Storage Mater.* **2018**, *10*, 85−91.
(28) Liu, F.-Q.; Wang, W.-P.; Yin, Y.-X.; Zhang, S.-F.; Shi, J.-L.; Wang, L.; Zhang, X.-D.; Zheng, Y.; Zhou, J.-J.; Li, L.; Guo, Y.-G. Upgrading Traditional Liquid Electrolyte via In Situ Gelation for Future Lithium Metal Batteries. *Sci. Adv.* **2018**, *4*, No. eaat5383.
(29) Hoyle, C. E.; Bowman, C. N. Thiol-Ene Click Chemistry. *Angew. Chem., Int. Ed.* **2010**, *49*, 1540−1573.
(30) Cramer, N. B.; Bowman, C. N. Thiol-Ene and Thiol-Yne Chemistry in Ideal Network Synthesis. In *Thiol-X Chemistries in Polymer and Materials Science*; Lowe, A. B., Bowman, C. N., Eds.; The Royal Society of Chemistry, 2013; pp 1−27.
(31) Wood, K. N.; Kazyak, E.; Chadwick, A. F.; Chen, K.-H.; Zhang, J.-G.; Thornton, K.; Dasgupta, N. P. Dendrites and Pits: Untangling the Complex Behavior of Lithium Metal Anodes through Operando Video Microscopy. *ACS Cent. Sci.* **2016**, *2*, 790−801.
(32) Zheng, Q.; Ma, L.; Khurana, R.; Archer, L. A.; Coates, G. W. Structure-Property Study of Cross-Linked Hydrocarbon/Poly-(Ethylene Oxide) Electrolytes with Superior Conductivity and Dendrite Resistance. *Chem. Sci.* **2016**, *7*, 6832−6838.
(33) Zeng, X.-X.; Yin, Y.-X.; Li, N.-W.; Du, W.-C.; Guo, Y.-G.; Wan, L.-J. Reshaping Lithium Plating/Stripping Behavior via Bifunctional Polymer Electrolyte for Room-Temperature Solid Li Metal Batteries. *J. Am. Chem. Soc.* **2016**, *138*, 15825−15828.
(34) Fetters, L. J.; Lohse, D. J.; Richter, D.; Witten, T. A.; Zirkel, A. Connection between Polymer Molecular Weight, Density, Chain Dimensions, and Melt Viscoelastic Properties. *Macromolecules* **1994**, *27*, 4639−4647.
(35) Zhao, Q.; Liu, X.; Stalin, S.; Khan, K.; Archer, L. A. Solid-State Polymer Electrolytes with in-Built Fast Interfacial Transport for Secondary Lithium Batteries. *Nat. Energy* **2019**, *4*, 365−373.
(36) Pei, A.; Zheng, G.; Shi, F.; Li, Y.; Cui, Y. Nanoscale Nucleation and Growth of Electrodeposited Lithium Metal. *Nano Lett.* **2017**, *17*, 1132−1139.
(37) Deng, Y.; Zheng, J.; Warren, A.; Yin, J.; Choudhury, S.; Biswal, P.; Zhang, D.; Archer, L. A. On the Reversibility and Fragility of Sodium Metal Electrodes. *Adv. Energy Mater.* **2019**, *9*, 1901651.
(38) Cogswell, D. A. Quantitative Phase-Field Modeling of Dendritic Electrodeposition. *Phys. Rev. A: At., Mol., Opt. Phys.* **2015**, *92*, 011301.

https://dx.doi.org/10.1021/acs.macromol.0c00475
Macromolecules 2020, 53, 5445−5454

(39) Zheng, J.; Engelhard, M. H.; Mei, D.; Jiao, S.; Polzin, B. J.; Zhang, J.-G.; Xu, W. Electrolyte Additive Enabled Fast Charging and Stable Cycling Lithium Metal Batteries. *Nat. Energy* **2017**, *2*, 17012.

https://dx.doi.org/10.1021/acs.macromol.0c00475
Macromolecules 2020, 53, 5445−5454